Bulletin of Earthquake Engineering (2021) 19:2817–2838
https://doi.org/10.1007/s10518-021-01091-3

ORIGINAL ARTICLE

Sand-granulated rubber mixture to prevent liquefaction-induced uplift of buried pipes: a shaking table study

Nurhan Ecemis[1] · Hadi Valizadeh[1] · Mustafa Karaman[1]

Received: 31 August 2020 / Accepted: 29 March 2021 / Published online: 5 April 2021

Abstract
Buried pipelines in liquefiable soils are vulnerable and can float during earthquake excitation. The uplift forces due to pore-water-pressure generation relocate the pipelines in the soil. Therefore, it is essential to measure the liquefaction effects of the backfill materials on buried pipes and make an intelligent choice for the surrounding soil to reduce the applied forces on pipelines during liquefaction. Recently, scrap tire–soil mixtures have been used as a new geomaterial to decrease the adverse effects of liquefaction. This paper investigates the flotation of the buried pipe and the sand–granulated rubber mixture's effectiveness around the pipe by a series of shaking table tests. Dynamic tests were performed under 1 g conditions on a fully saturated sand–granulated rubber mixture with small-diameter buried pipes. Three different granulated-rubber dimensions of 2.5–5, 5–10, and 10–15 mm and granulated rubber ratios of 10, 20, and 30 percent were examined in the tests. The outcomes of excess pore water pressure, settlement, pipe uplift, and upward pressure during and after shaking were compared. The test results demonstrated that the sand–granulated rubber mixture reduces excess pore water pressure accumulation and prevents liquefaction. Moreover, the effect of pipe diameter, burial depth, consolidation coefficient of the mixture, and uplift initiation time on pore water pressure and load increment below the pipe were combined to predict the buried pipe's uplift probability.

Keywords Shaking table test · Sand-granulated rubber mixture · Pore water pressure · Liquefaction · Buried pipes uplift

1 Introduction

Embedded pipelines are vital energy services that transfer gas, petroleum, water, and sewage throughout subterranean urban and non-urban landscapes. It has been observed from past earthquakes that permanent ground deformation, resulting from liquefaction-induced lateral spreading, is a significant seismic hazard that may cause substantial damage to

✉ Nurhan Ecemis
nurhanecemis@iyte.edu.tr

[1] Civil Engineering Department, Izmir Institute of Technology, Urla, 35430 Izmir, Turkey

pipelines. In addition, during liquefaction, pipes buried at shallow depths are subjected to excess pore water pressure, which causes uplift of the pipes. Numerous researchers have reported damage to buried pipelines due to liquefaction at the ground by several major earthquakes (e.g. Hall and O'Rourke 1991; Mohri et al. 1995; Hamada et al. 1996; O'Rourke and Liu 1999).

In recent years, several methods have been recommended to avoid the uplift of buried pipes during liquefaction (Orense 2015). However, how these techniques perform in terms of liquefaction mitigation for buried pipelines is less well known. Mohri et al. (1999) placed gravels above the pipe to resist flotation by increasing the dead weight. Gravels and geosynthetic materials were also applied around large-diameter buried pipes by Ling et al. (2003). The usage of these countermeasures reduced the pipe uplift by about 10 percent. Zou et al. (2006) compared the impact of different surface-gravel drain shapes. Castiglia et al. (2019) performed four shaking table tests to study the effectiveness of gravel bags placed above and below the pipe to increase the stability of pipelines subjected to uplift in liquefiable soils. Moreover, Castiglia et al. (2020) used geogrid sheets as a remedy for the liquefaction-induced uplift of buried pipelines.

The amount of waste tires produced worldwide is tremendous, at over 1 billion, and it increases each year (Thomas and Gupta 2015). Therefore, reinforcing soil with scrap tire–derived materials is an economically feasible alternative method to using gravel to avoid the flotation of shallowly buried pipelines due to liquefaction. Scrap tire–derived materials have been used as geomaterials in the form of soil–tire mixtures since 1990, mainly in the United States. The tires are cut into different sizes and shapes, depending on the intended use, and classified as granulated rubber (GR), crushed rubber, powdered rubber, rough shred, tire chips, tire-derived aggregate, and tire shreds (ASTM D 6270–08, 2012).

Recently, several researchers have proposed reinforcing soil with scrap tire–derived materials for liquefaction mitigation purposes. Youwai and Bergado (2003) conducted triaxial tests on sand–tire mixtures to investigate their mechanical behavior. They found that the addition of tires reduced the shear strength and increased the failure strain of the mixture. Zornberg and Cabral (2004) investigated the effect of shredded tire content on the tire–sand mixture's function using a large-scale triaxial device. Gotteland et al. (2005) performed an element test on tire–sand mixtures to assess their mechanical behavior. According to the results, the tire content dramatically influenced the shear strength of the mixture. Several direct shear tests on sands with different percentages of tire-shred content were carried out by Attom (2006). The results showed that the shear strength and friction angle increased with shredded tire increments. Uchimura et al. (2007) performed several shaking table tests on buried pipes in a tire chip–sand mixture with different tire chip contents. They realized that the sand–tire chip layer around the pipes could relieve the uplift of buried pipes and diminish the excess pore water pressure ratio. Uchimura et al. (2008) compared clean sand and tire–derived aggregate-sand mixtures under cyclic loading. They inferred that tire-derived aggregate-sand mixtures required more cycles to reach liquefaction and exhibited smaller axial strains than clean sand did.

Hazarika et al. (2010) conducted both shaking table and cyclic triaxial tests to study the effect of reinforced sand with tire chips on the liquefaction susceptibility and displacement of quay walls. The results demonstrated that the excess pore water pressure ratio decreased with the tire chips' volumetric ratio. In addition, the residual displacement of the quay wall decreased in the reinforced case. Kaneko et al. (2013) studied the seismic isolation effects of tire chips and their effectiveness as a remedy for saturated sand liquefaction during earthquakes. They showed that a significant damping ratio and dynamic isolation effects

could be detected when tire chips were mixed with sand. Neaz Sheikh et al. (2013) concluded that the presence of tire scraps significantly affected the ultimate shear strength and the corresponding axial strain of sand.

Bahadori and Manafi (2014) investigated the effect of tire chip contents on liquefiable sand deposits using a series of shaking table tests. The results showed that using an increase in tire chip percentage reduces pore water generation due to liquefaction. The mean damping ratio increased with an increasing tire chips ratio in the mixture. Noorzad and Raveshi (2017) performed triaxial tests to investigate the behavior of the sand–tire chip mixtures. The results showed that the shear strength of the mixtures decreased with the increase in the number of tire chips. This result contradicts the results of some previous studies in which tire chips increased the shear strength of sand–tire mixtures.

Based on previous studies, it is evident that the behavior of the tire–soil mixture as a backfill material is still a concern because the mechanics of tire–soil mixtures are still not fully understood. Therefore, additional large-scale model tests are necessary to further investigate the dynamic properties of the sand–GR (SGR) mixture and its effectiveness on the flotation of buried pipe. On this basis, a series of 1 g shaking table tests was carried out on a fully saturated SGR mixture with small-diameter buried pipes. In particular, the influences of GR on liquefaction and the resulting deformations were explored. GR has more flexibility in terms of reducing the stress concentration, compressibility, and porosity than sand particles do (Edil and Bosscher 1994; Hyodo et al. 2008). Therefore, the use of GR along with sand particles is beneficial for liquefaction mitigation. However, rubbers still maintain their lightweight ability (low specific gravity of 1.17). It is also essential to determine the uplift pressure on buried pipelines to assess the pipeline flotation potential for various SGR mixtures. Therefore, the backfill and pipe density should be sufficient to balance the developed uplift forces on buried pipelines during earthquakes. A better understanding of uplift forces development during liquefaction will enable a more appropriate pipeline design.

2 Description of the proposed material for mitigation

In this study, fine silica sand mixed with scrap GR was used as a backfill material around the pipe. The sand particles were naturally formed grains that were supplied locally. The relative density (G_s), minimum void ratio (e_{min}), and maximum void ratio (e_{max}) of silica sand were 2.61, 0.60, and 0.79, respectively. A local shredding company offered the scrap rubber, and most of the metals and fibers were removed beforehand. The particle-size distribution curves of clean sand, different-sized GR, and SGR mixtures are shown in Fig. 1a. The soil was determined as poorly graded sand (SP), based on the Unified Soil Classification System.

Three GR dimensions of 2.5–5 mm, 5–10 mm, and 10–15 mm were used to obtain the SGR mixture backfill material for experiments. Samples of the silty sand and different sizes of GR used in the experiments are shown in Fig. 1b. According to ASTM D6270-08 (2012), the scrap rubbers used in this research comprise the GR size (non-spherical and < 0.425 mm to 12 mm). The GR dimension has an essential effect on the mechanical response of the mixtures, which can cause either decay in strength and maximum shear modulus (Anastasiadis et al. 2012; Lee et al. 2010) or an increase in strength and maximum shear modulus (Kim and Santamarina 2008).

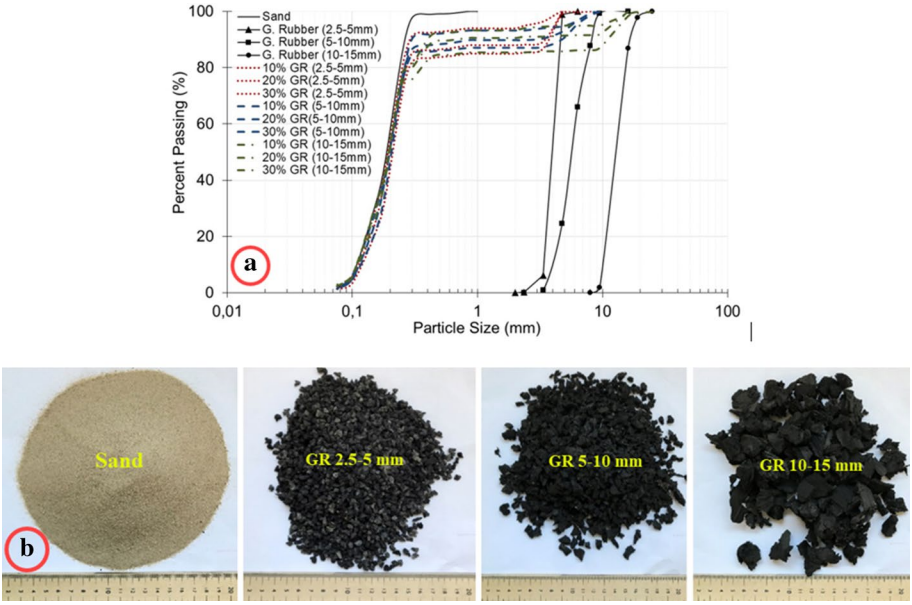

Fig. 1 **a** Particle size distribution of the sand, GR and SGR mixtures used in the experiments, and **b** sample of silty sand and GR (2.5–5 mm, 5–10 mm, 10–15 mm) used around the pipes in the experiments

The rubber grounds were found to be efficiently compressed by hand. They are three times more compressible than soil (CEN Workshop Agreement 2002). Therefore, sand-only backfill is stiffer than the compacted mixture. This issue decreases the buried pipes' damaging possibility in several circumstances, such as backfill compaction and possible non-uniform ground displacement. The average unit weight of GR with a 2–20 mm size and no compaction (loose state) is approximately 4–5.2 kN/m^3 (Manion and Humphrey 1992; Terzi et al. 2015). Based on ASTM D6270 (1998), in a loose state, the density of rubber ranges from 3.3 to 4.8 kN/m^3. Here, the saturated unit weight of the GR was found to be 5 kN/m^3, which is reasonably lightweight compared with the geomaterials. Figure 2 depicts the sand particles' shapes and individual rubber ground by the scanning electron

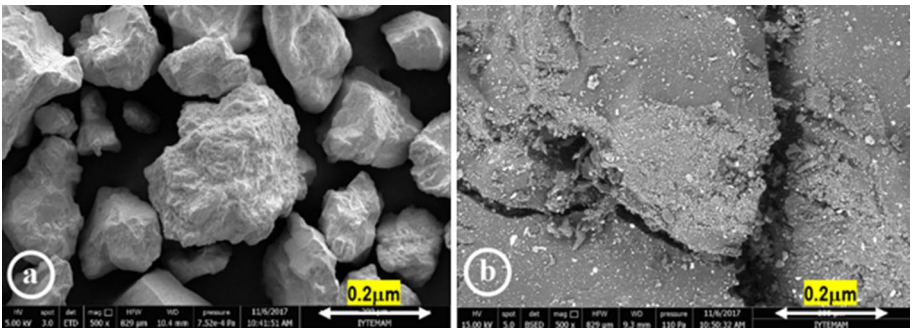

Fig. 2 Scanning electron micrograph of **a** sand particles, and **b** tire ground used in the shaking table tests

microscope. Based on microscopic inspection, the sand particles and rubber grounds have a subangular and rough surface, respectively.

The grain-size properties, as well as the specific gravity (ASTM D854-14) of the sand particles and different-size rubber grounds used in this study, are listed in Table 1. The bulk and specific-gravity values of tire shreds were 0.98–1.06 and 1.02–1.27, respectively (ASTM D6270, 1998), compared with the values of 1.13–1.36 reported by Edil and Bosscher (1994). The specific gravity of the GR used in the experiments was determined as 1.17, representing only 45 percent of the particle density of the silica sand used in the experiments (Table 2). This specific-gravity value is similar to the result obtained by Promputthangkoon and Hyde (2010).

3 Experimental program

3.1 Shaking table tests

A series of 13 shaking table tests was performed to investigate the liquefaction effects on the SGR mixture on small-diameter pipes. The laminar box, which can simulate in situ free field conditions, was fixed to a 2×1 m shake table with one degree of freedom. The laminar box used in the experiments comprised 24 stacked rings (called laminates), which were factory made from aluminum alloy. They were preferred to eliminate the inertial effects of laminates on the soil movements. These rings were separated and supported by steel rollers mounted between each laminate to considerably decrease friction between the layers. The internal sizes of the box were 163 cm (length) by 45 cm (width) by 150 cm (height). A rubber membrane was used to restrain the saturated deposit in the laminar box. The thickness of the membrane was chosen as 1 mm to avoid affecting the movement of the laminar box. The performance of this box containing the soil was reported in a separate paper (Ecemis 2013).

3.2 Specimen preparation

The GR ratio was evaluated as the ratio of the GR dry volume to the total mixture volume. The mixtures were produced using GR ratios of 0, 10, 20, and 30 percent for three dimensions (2.5–5 mm, 5–10 mm, and 10–15 mm). The sample of different-sized GR (20 percent by volume) with sand is shown in Fig. 3b. Figure 1a illustrates the particle-size distribution curves of the SGR mixtures, with the fine percentage by weight in the vertical axis. The grain-size characteristics of the SGR mixtures are similar to pure sand because of the lightweight nature of GR. Table 1 shows the physical properties of the SGR mixtures used in the experiments.

A 65 cm high, fully saturated silica sand deposit was placed into the box by the hydraulic filling technique, allowing sand grains to sink slowly through the water and simulating the process of alluvial deposition of soils in rivers/lakes. To densify the soil, the laminar box was shaken with various accelerations for several minutes. This 65 cm high dense-sand layer represents the non-liquefiable original ground. Then, above the dense-sand layer, the dry SGR mixture at a prescribed ratio by volume was poured steadily from a shallow height to avoid segregation and create a uniform, loosest mixed composite inside the laminar box. As Mahboub and Massie (1996) reported, particle segregation is an expected problem for mixtures using two materials, with a significant

Table 1 Physical properties of SGR mixtures and specification of models for shaking table tests

Test no	Instrument Layout	GR ratio (by volume)	GR ratio (by weight)	GR dimension	D_{10}	D_{50}	C_u	C_c	γ_{sat}	D_r^*	Pipe
–	–	(%)	(%)	(mm)	(mm)	(mm)	–	–	(kN/m^3)	(%)	–
T1	Figure 6a	0	0	–	0.12	0.19	1.71	0.91	20.90	33	Free pipe
T2		0	0	–	0.12	0.19	1.71	0.91	20.50	49	
T3		0	0	–	0.12	0.19	1.71	0.91	20.90	24	
T4	–	0	0	–	0.12	0.19	1.71	0.91	20.90	37	No pipe
T5	Figure 6b	10	6.76	2.5–5	0.11	0.2	2.0	1.31	19.27	26	Fixed/Free pipes
T6		20	10.12	2.5–5	0.11	0.2	2.0	1.34	19.16	35	
T7		30	14.35	2.5–5	0.12	0.2	1.91	1.28	18.65	39	
T8		10	4.74	5–10	0.12	0.2	1.83	1.23	20.08	29	
T9		20	9.08	5–10	0.11	0.2	2.10	1.18	19.47	42	
T10		30	13.46	5–10	0.11	0.2	1.91	1.11	18.55	28	
T11		10	6.43	10–15	0.11	0.2	1.91	1.28	20.08	10	
T12		20	11.95	10–15	0.11	0.2	2.0	1.31	19.37	41	
T13		30	13.77	10–15	0.11	0.2	2.0	1.02	17.94	20	

GR Granulated Rubber, *γsat* Saturated unit weight, D_r Average initial relative density for the loose layer (*CPT Results), D_{10} Effective particle size D_{50} Mean grain size of the particle, C_u Coefficient of uniformity, and C_c Coefficient of curvature

Table 2 Summary of the shaking table tests

Test #	Frequency (Hz)	Input max. disp. (mm)	a_{max} (g)	Duration (s)
T1	2	12.45	0.2	20
T2	2	22.54	0.35	20
T3	2	26.89	0.46	20
T4-13	2	22.54	0.35	20

a_{max} maximum acceleration

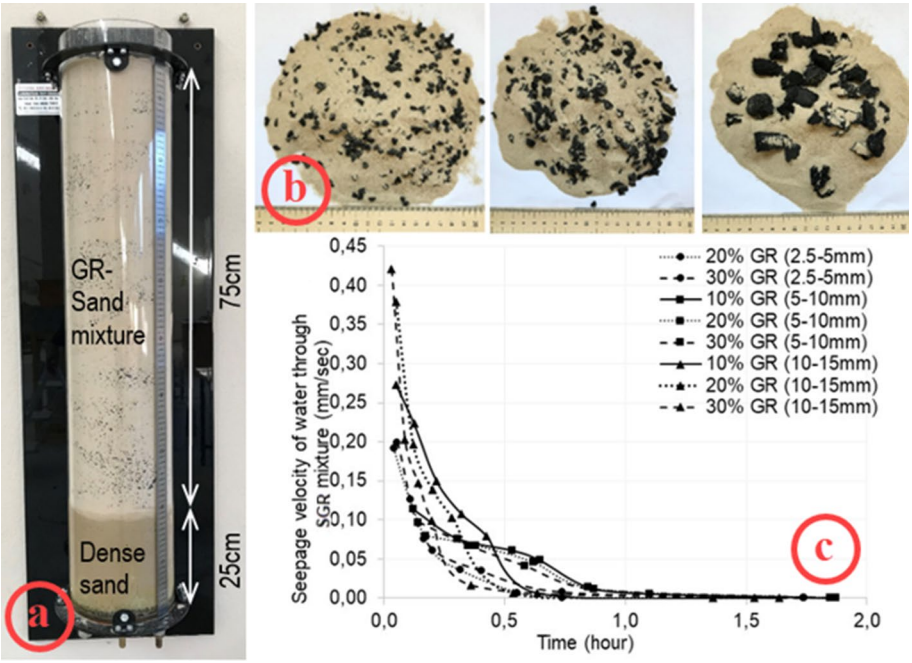

Fig. 3 **a** Cylindrical cell calibration model to verify the deposition of the fully saturated SGR mixture in the laminar box, **b** sand mixed with 3–5 mm, 5–10 mm, 10–15 mm GR (20 percent by volume), and **c** seepage velocity of water through SGR mixture

difference in specific gravity. However, in all tests, no evidence of segregation was observed for comparatively high sand contents (more than 70 percent). Edil and Bosscher (1994) and Bosscher et al. (1992) also found that, when the amount of sand was more than 30 percent based on volume, the sand contents remained unsegregated. The first 10-cm-deep SGR mixture was placed at a prescribed ratio by volume, and then a model of buried pipe was introduced. Then, the box continued to be filled with a 65 cm deep SGR mixture. After the dry sand-tire chips mixture was established, water was carefully added to the mix to obtain a fully saturated deposit.

The saturated unit weight of the mixture throughout the depth was measured by cylindrical buckets. The small buckets were located inside the SGR mixture at four different depths throughout the preparation of each soil deposit; the buckets were removed when they were filled with the mixture. Table 1 presents the average saturated density of the mixture throughout the depth.

A series of calibration tests was conducted in a cylindrical cell with an inside diameter and height of 19 cm and 105 cm to prepare a fully saturated mixture in the laminar box. As shown in Fig. 3a, the first 25-cm-high fully saturated dense sand layer was placed in the cylindrical cell. Above the dense sand layer, a 75-cm-deep SGR mixture at a prescribed ratio was established. Then, water was added slowly from the top of the cylindrical cell to saturate the SGR mixture. The slow process of saturation insured that the deposit was not disturbed. At the end of saturation, the water level was retained 1 cm above the soil surface. Figure 3c shows the duration of saturation for different GR diameters and GR ratios. For each mixture, a typical saturation process took less than around 1.5 h. Therefore, for the full saturation process of the mixture deposits inside the laminar box, the water was filled slowly, and the sample was left quietly for at least 2 h.

3.3 Cone penetration test

Before the shaking table tests, cone penetration tests (CPTs) were performed to determine the mixture and clean sand layer stiffness throughout the depth. As shown in Fig. 4, the 60° tapered, 10 cm^2 tip area probe (D = 3.57 cm) penetrated the soil at a continuous penetration velocity of 2 cm/s (ASTM D3441 2016) using a hydraulic pump. The position of the cone penetration on the ground surface is displayed in Fig. 4c. The CPTs provided measurements of cone penetration resistance (q_c) and friction resistance (f_s) for each 1 cm of penetration throughout the depth. The measured data were digitized inside the probe and then transferred acoustically to the data-acquisition system. Figure 5 displays the measured q_c profiles of the sample versus the depth. As shown, the q_c values exhibited a sudden increase after a depth of 0.75 m, which corresponds to the non-liquefiable dense sand layer. Above a depth of 0.75 m, the q_c values were uniform and significantly smaller than at the bottom, corresponding to the loose SGR mixture. These results indicate that the deposition method showed success in terms of the uniformity and stiffness of cone-tip resistance throughout the mixture and the clean sand layers. The relative density throughout the soil depth was determined from the measured CPT resistance using the correlation given by Lunne et al. (1997). The relative density reported in Table 1 for each test sample was obtained from the average amount of the initial relative density for the loose upper layer.

The main and important factor affecting the CPT measurements in the box is the ratio of the diameter of the box to the CPT probe (R_d). Several researchers (Phillips and Valsangkar 1987; Renzi et al. 1994) have investigated the effects of boundaries on cone penetration data, and whether the boundary conditions of the box can model the in situ free field conditions. Phillips and Valsangkar (1987) and Renzi et al. (1994) stated that the side-boundary effects are negligible, even when the cone probe is positioned at a distance from the boundary corresponding to $R_d = 5$ and $R_d = 11$, respectively. As shown in Fig. 4c, CPT tests were performed along a concentric circle (diameter = 45 cm). The distance of the cone to the wall offers an R_d value of 13. This confirms that the boundary conditions of the box can sufficiently model the in situ free field conditions.

3.4 Test process and instrumentation

All the tests performed are outlined in Table 1. In tests T1 to T3, a pipe with only free-ends was installed inside the loose clean sand to investigate the effect of the acceleration level on buried pipelines. The plan and side views of the free-ends pipe configuration and instrument layout for tests T1 to T3 are shown in Fig. 6a. In test T4, no pipe was

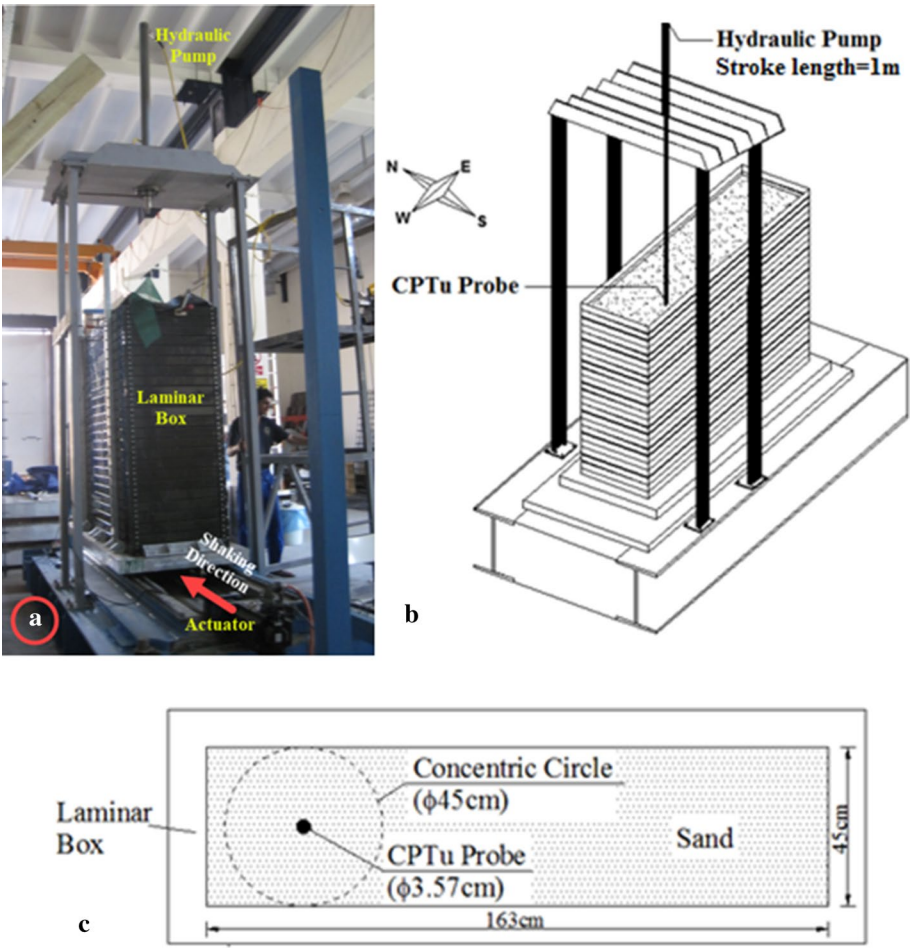

Fig. 4 **a** Photo of the CPT system, **b** schematic view of the cone-penetration system, and **c** position of penetration in the soil deposit

installed. In tests T5 to T13, at the same acceleration level, both the fixed and free-ends pipes were placed in the SGR mixture to observe the effects of the mixture on the buried pipe reaction during and after the liquefaction. The plan and side views of both the fixed and free-ends pipe configurations and instrument layouts for tests T5 to T13 are shown in Fig. 6b.

As illustrated in Fig. 6a–b, at each test, one potentiometer (X-P1) for measuring lateral movement was installed on the shake table. In addition, five piezometers (PP1–PP5) for determining the pore water pressure (Δu) were placed at different depths of the SGR mixture. Two accelerometers (SA1 and SA2) were positioned inside the soils at the same level as the pipes. Two other potentiometers (Z-P1 and Z-P4) were positioned on the ground surface to monitor surface displacement during and after shaking. The potentiometers recorded the surface settlements attached to the settlement plate that were laid parallel on the soil surface. The plate's mass was chosen as liquefied soil to provide equal plate and soil movement during testing. Z-P1 and Z-P4 were placed 25 cm and 65 cm away from the

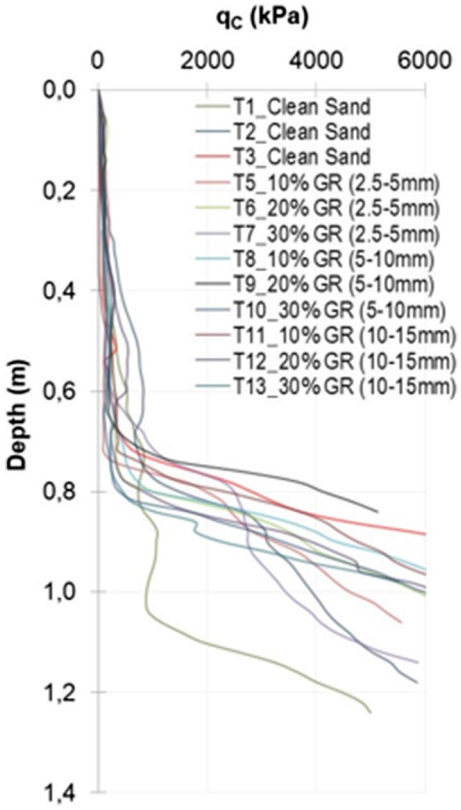

Fig. 5 Cone penetration resistance (q_c) versus depth (CPT Results)

free pipe center, respectively. The data were recorded with a typical reference timeframe and time interval using the data acquisition system.

3.4.1 Pipe configuration

Although there is a great range in pipe diameter, the experimental portion of this study focuses on small-diameter local gas pipelines. In practice, these pipes are typically buried in the top 1.5 m of the soil surface below the groundwater level. Therefore, based on the model dimensions, polymeric plastic pipes were used; they were made of polyvinyl chloride with an external diameter of 50 mm, thickness of 1.8 mm, and length of 385 mm. The elasticity modulus and Poisson's ratio of the pipe material were 3,316 MPa, and 0.40, respectively. The unit weight, ultimate tensile strength, and bending strength of the pipe material were 13.83 kN/m^3, 52 MPa, and 88 MPa, respectively.

Two potentiometers (Z-P2 and Z-P3) were attached to the free pipe by wires to detect pipe uplifting (Fig. 7a). Three miniature load cells (EP1, EP2, and EP3), with a capacity of 200 kPa, were pasted at the outside bottom face of the fixed pipe to measure the earth pressure (normal stress) developed on the pipe during and after shaking (Fig. 7b). The fixing of the pipe was intended to avoid the uplift. Two ends of the pipe were sealed with a plastic damper to prevent the entry of sand particles and reduce friction between the pipe and the sidewalls. The free pipe mass, including the transducers, rods, and rails, was 2.4 kg. The

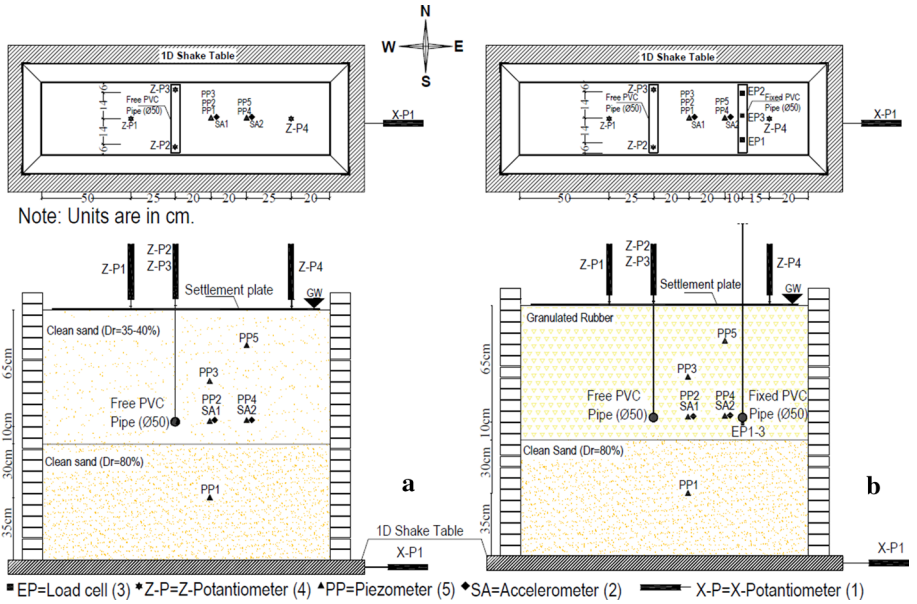

Fig. 6 Configuration of model pipes within the test apparatus and the schematic sketch of instrumentation on the pipe, shake table and saturated SGR mixture deposit for tests **a** T1-T3, **b** T5-T13

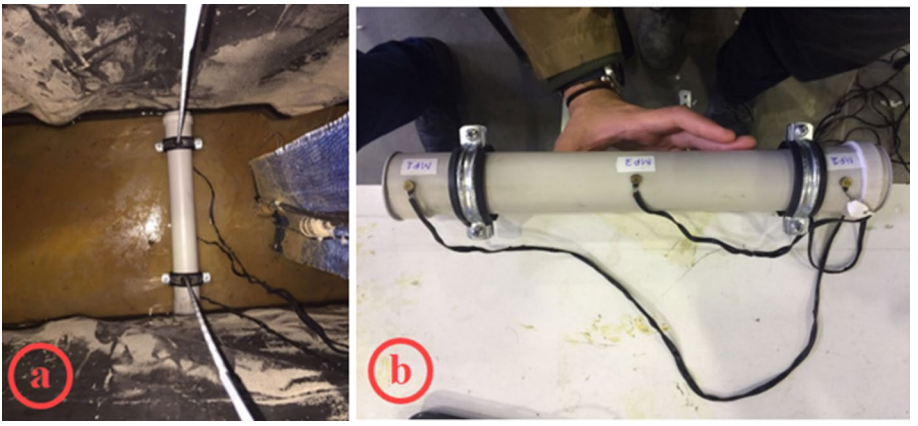

Fig. 7 **a** Free pipe model with attached potentiometers, and **b** fixed pipe model with attached load cells

strains of the pipe were not examined in the experimental program because flotation of the pipe was the key matter.

3.4.2 Effect of maximum acceleration on backfill and assessment of liquefaction

The effect of maximum acceleration on clean sand backfill and pipe response was examined by comparing the results of tests T1, T2, and T3. In these tests, three different

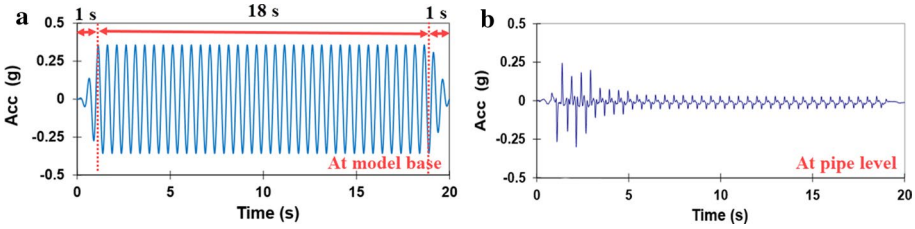

Fig. 8 The acceleration time-histories **a** at the model base, and **b** pipe level (a_{max} = 0.35 g)

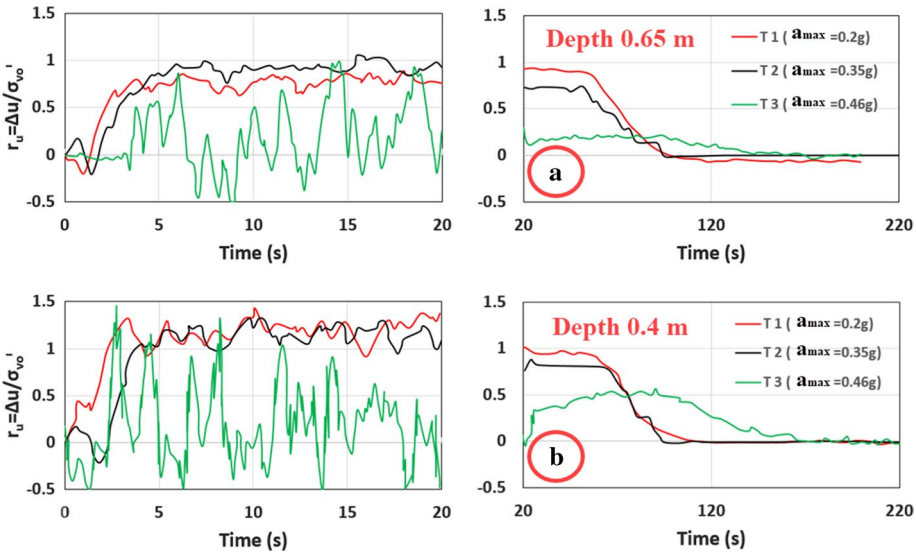

Fig. 9 The Δu ratio of sand deposit for a_{max} 0.2 g (T1), 0.35 g (T2), and 0.46 g (T3) at depths **a** 0.65 m, and **b** 0.4 m

maximum horizontal accelerations, a_{max} (0.2 g, 0.35 g, and 0.46 g) with 2 Hz frequency, were applied. This frequency was selected to control the shaking system (Ecemis 2013; Ecemis et al. 2015). The applied accelerations were sinusoidal and unidirectional, with a constant frequency. These accelerations were generally increased from zero to maximum level, a_{max}, in 1 s, and then a_{max} was continued for 18 s. Finally, a_{max} was slowly reduced back to zero over 1 s, as shown in Fig. 8a. The measured accelerations at the pipe level (burial depth of 0.65 m) for test T2 are shown in Fig. 8b. As illustrated in the figure, the wave weakened at the pipe level as the soil liquefied. The acceleration during the initial few shaking cycles was large, and after liquefaction, the acceleration reduced. The changes in the excess pore water pressure ratio at 0.65 m and 0.4 m in depth during and after shaking tests T1, T2, and T3 are given in Figs. 9a–b. At each depth, Δu results with oscillation were observed for test T3 (with a_{max} = 0.46 g). Therefore, the maximum ground acceleration of a_{max} = 0.35 g was used in the subsequent shake table tests (tests T4 to T13), based on the difficulty of controlling the laminar box deformation for a_{max} = 0.46 g in the laboratory condition and oscillation measured from the Δu results.

In this study, the pore pressure ratio (r_u), which is the ratio of excess pore water pressure (Δu) to the initial effective vertical stress (σ_{vo}'), was used to assess the full liquefaction. In general, liquefaction occurs when $r_u = \Delta u/\sigma_{vo}'$ reaches a threshold value of 1.0. However, because of dislocation of the piezometers or a change in the water table elevation (Ecemis 2013), the Δu ratio was found to be slightly more or less than 1.0. For example, the σ_{vo}' values at a depth of 0.65 m were 6.9, 6.9, and 5.7 kPa for tests T1, T2, and T3, respectively. As shown in Fig. 9a, the peak r_u values at this depth reached 0.9 ($\Delta u = 6.12$ kPa) and 1.0 ($\Delta u = 7.3$ kPa) for tests T1 and T2, respectively. As clearly shown in the pore pressure dissipation results of test T2, the generated excess pore pressure essentially dissipated in the post-shaking stage, and the pore pressure ratio had returned to zero (Fig. 9a). However, in test T1, the pore pressure ratio did not return to zero. Instead, at the end of the dissipation, the Δu ratio returned to− 0.1. Although the peak r_u appeared as 0.9, by adding 0.1 to the peak value, it is possible to state that full liquefaction occurred during test T1 with a value of r_u almost equal to 1.0.

The σ_{vo}' values at a depth of 0.4 m were obtained 3.7 kPa for tests T1, T2, and T3. As shown in Fig. 9b, the peak r_u values at a depth of 0.4 m reached 1.4 ($\Delta u = 5.21$ kPa) and 1.3 ($\Delta u = 4.9$ kPa) for tests T1 and T2, respectively. For tests T1 and T2, the r_u values found were remarkably larger than 1.0. This discrepancy may have arisen because of the settlement of the piezometers or a rise in the water table elevation (Ecemis, 2013).

3.4.3 Effect of pipe's presence on liquefaction

Figure 10 shows the response of $r_u = \Delta u/\sigma_{vo}'$ in the clean sand deposit when there is no pipe (T4) and pipe buried in the soil (T2). In the soil deposit with and without the pipe, r_u at depths of 0.4 m and 0.65 m gave a ratio close to unity, which implied full liquefaction. With the presence of a pipe in the soil, the pore pressure generation and dissipation did not respond similarly.

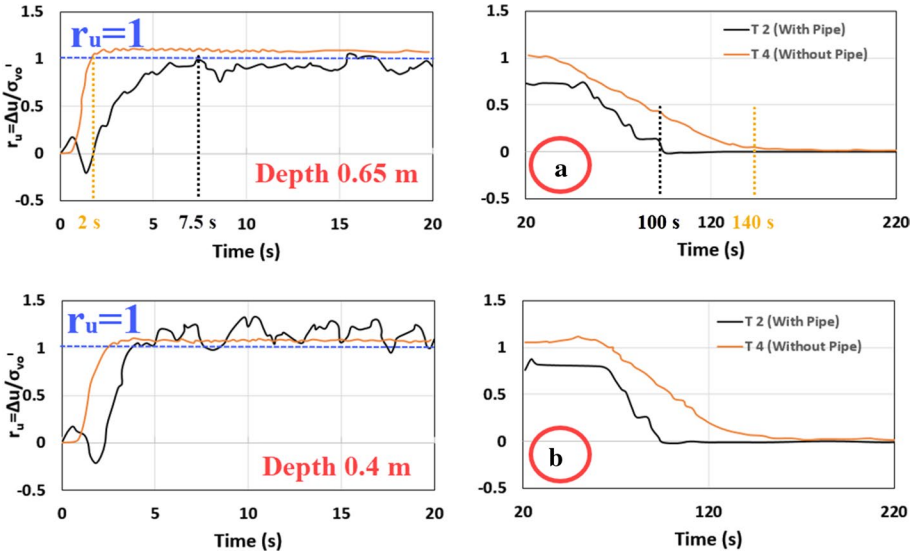

Fig. 10 The generation and dissipation of excess pore pressure of sand deposit with no-pipe (T4) and pipe (T2) buried at **a** 0.65 m, and **b** 0.4 m depth

It should be noted that the Δu of the backfill generated slowly and dissipated more quickly when the pipe was in the backfill. With the shaking initiation, in test T2, r_u reached unity in about 7.5 s. The time for the sample to reach liquefaction without a pipe was 2 s. For the soil where pipes were not installed (T4), the dissipation took more than 140 s (Fig. 10). By the end of the shaking, the pore water pressure dissipated rapidly in test 2 (with a pipe) for about 100 s (Fig. 10). These results imply that there was water flow surrounding the pipe and the quick dissipation of pore water pressure occurred in test T2 because of the pipe uplift.

4 Test observations: effect of the GR dimension and ratio

The shaking table tests were conducted on pipes surrounded by an SGR mixture (T5–T13) to investigate the GR dimension and ratio effect on the pipe uplift induced by the liquefaction. The SGR mixture enhanced the water flow near the pipe, mitigated the liquefaction of the mixture, and sped up the pore water pressure dissipation. Table 3 summarizes the essential values needed to compare the tests with this mitigation technique.

4.1 Excess pore pressure generation and pressure increment on the pipe

The generation of $r_u = \Delta u/\sigma_{vo}'$ at the pipe level (0.65 m in depth) obtained from different ratios and sizes of the SGR mixture is shown in Fig. 11a. At the same depth, the inclusion of light rubbers in the mixture caused smaller initial effective stresses (σ_{vo}') compared with the clean sand. For each test layer, the σ_{vo}' values are indicated in Table 3.

In test T2, where clean sand was placed, the r_u rose to 1.0 at around 7.5 s. Eventually, r_u approached an almost constant value. This indicates a large reduction in the effective stress in the sand-only backfill. For other tests consisting of different amounts and sizes of GR in the sand, the Δu responded differently. In the SGR mixture, Δu increased slowly to a much lower amount. In the case of each GR dimension and ratio, according to average r_u values, no liquefaction occurred. For the GR dimension of 2.5–5 mm and GR ratio of 10, 20, and 30 percent, the average r_u values were 0.8, 0.82,

Table 3 GR dimension and ratio impacts on liquefaction mitigation

Test #	GR dimension (mm)	GR ratio (%)	$(\Delta u)_{avg}$ (kPa)	σ_{vo}'(kPa)	$(r_u)_{avg}$	Pipe Uplift* (mm)
T2	–	–	6.58	6.93	0.95	38.16
T5	2.5–5	10	4.73	5.91	0.80	16.73
T6		20	4.80	5.85	0.82	35.97
T7		30	3.71	5.70	0.65	14.22
T8	5–10	10	4.05	6.42	0.63	45.18
T9		20	4.53	6.04	0.75	22.58
T10		30	3.11	5.46	0.57	70.25
T11	10–15	10	–	6.41	–	48.53
T12		20	–	5.97	–	28.87
T13		30	–	5.70	–	41.84

*Average uplift values obtained for stage II

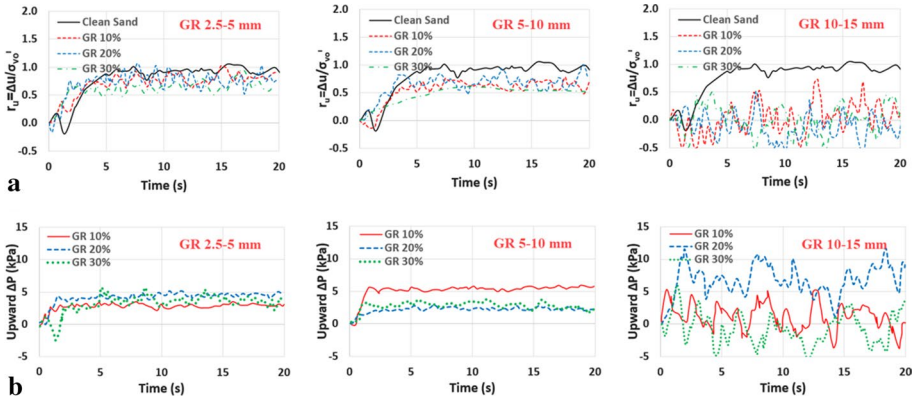

Fig. 11 Time histories of **a** excess pore water pressure ratio at the side of the pipe, and **b** load increment at the bottom of the fixed pipe

and 0.65, respectively. For the GR dimension of 5–10 mm and GR ratio of 10, 20, and 30 percent, the average r_u values were 0.63, 0.75, and 0.57, respectively. In the samples with a GR dimension of 10–15 mm, impressive oscillation was observed in the r_u values. The result shows that the SGR mixture mitigated the liquefaction at the pipe level.

In the GR dimension of 10–15 mm, the Δu was not significantly generated during the shaking. This response may have been due to the larger particle dimension of the GR compared with the sand. Another possible reason may be the highly deformable (low stiffness) nature of GRs (Kaneko et al. 2013). In this explanation, instead of transferring the load between the GRs and the pore water, the rubbers deformed, and high Δu was not observed during shaking. The contact force and the friction between particles became more stable that with sand particles because the contacts are solid when the pore water pressure increases. However, the deformation in the particles may not recover considerably. The low specific gravity of rubbers can reduce the total density of the liquefied SGR mixture, which can cause a lower buoyant force to the pipe inside the backfill. These findings demonstrate the effectiveness of GRs in preventing the liquefaction phenomenon.

The earth pressure increments (ΔP) at the bottom of the fixed pipe during shaking are shown in Fig. 11b. The ΔP was almost the same as the generated Δu values at the sides of the pipe. For specimens with GR dimension of 2.5–5 mm, the miniload cells that measured the applied ΔP showed a positive pressure increment on the free pipe of about 3–5 kPa during shaking. For specimens with a 5–10 mm GR dimension, the measured pressure showed a positive increment on the pipe of about 2.5–5 kPa during shaking. As shown in the figure, for the 10–15 mm GR dimension at 10 and 30 percent GR ratios, the pressure increments on the pipe fluctuated, and positive and negative values were measured during the shaking. The results showed that the increase in pressure was less than 10 kPa during shaking. The measured total stress from the load transducers showed that the earth pressure acting at the pipe increased after liquefaction. These findings imply that the pressure increments are not only related to the Δu but also to the settlement of the mixture and movement of the pipe.

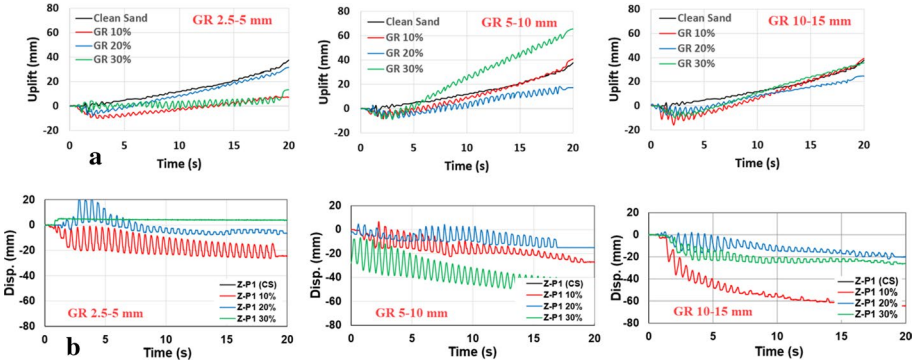

Fig. 12 Time histories of; **a** pipe uplifting during the shaking, **b** the mixture settlement (Z-P1)

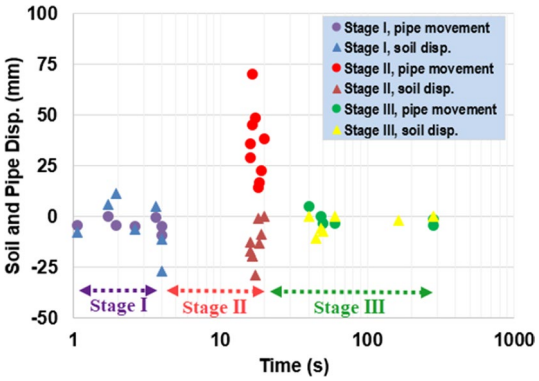

Fig. 13 The pipe and soil movement at stages I, II and III

4.2 Pipe uplifting and settlement of the mixture

The movement of the buried pipes and the SGR mixture settlement obtained from different GR dimensions and ratios are shown in Fig. 12a–b. The pipe movement was measured using two wires attached to the potentiometers. The vertical displacement on the ground surface was measured by two potentiometers attached to the settlement plate right above the pipe's sides. The potentiometer readings on the pipe indicated that the buried pipe in the sand-only backfill lifted up to 38 mm at the end of each shaking. The pipe in the backfill mixture showed settlement and reasonable uplift during shaking. Therefore, these cases were presented in three stages, and the illustration of these cases is given in Fig. 13. In each test, the recorded settlement of the pipes was between 0 and 10 mm up to 3 s of shaking. Meanwhile, the maximum recorded settlement of the mixture surface was about 35 mm. This was represented as stage I. During stage I, the change in Δu was not big enough to uplift the pipe (stage I, 0–3 s).

When Δu reached a threshold value, the pipe displacement changed, and uplift was seen for about 17 s during shaking (from 3 to 20 s). This was represented as stage II (stage II, 3–20 s). In each shaking test, the recorded uplift of the pipe was between 14 and 70 mm (Table 3), while the settlement recorded on the soil surface was around 0–29 mm. At the end of the shaking, pipe uplifting caused pore water pressure dissipation, and the pipe

settled by about 1–11 mm. At the same time, the maximum recorded settlement of the mixture was 10 mm. This was represented as stage III (stage III, 20–300 s). The pipe settlement at stages I and III was due to the soil settlement. As shown in Fig. 13, at stages I and III, the soil and pipe settled simultaneously. Although there was soil settlement in stage II, a pipe uplift was observed.

5 Compressibility and permeability effects of the mixture on pipe uplift behavior

The excess pore water pressure generation beneath the pipe and reduction of soil shear resistance resulted in the pipe flotation. However, no clear correlation was determined between the excess pore pressure ratio and pipe uplift at different GR dimensions and ratios. Based on the Δu time-history records, the excess pore pressure ratios at different GR dimensions and ratios are depicted in Fig. 11a. Instead of GR dimension and ratio, a combination of pipe diameter (D), burial depth (H), consolidation coefficient (c_h) of the mixture, and uplift initiation time (t) was used to develop a non-dimensional parameter (α), representing a wide range of situations, as follows:

$$\alpha = \frac{H \cdot D/t}{c_h} \tag{1}$$

where t is the uplift starting time ($t_{stage\ I}$). It is well known that the uplift starting time depends strongly on dynamic loading conditions. In this study, the dynamic loading conditions were constant. The only variable was the coefficient of consolidation (c_h), which was obtained from the pore water pressure dissipation results taken from the piezometers placed in the mixture. The c_h values between 8 and 16 cm^2/s were extracted from the dissipation tests. Figure 14a shows the variation in the upward pressure on the fixed pipe versus α, for a maximum acceleration of 0.35 g. The upward pressure was the maximum value measured during stage I. The increase in pore water pressure during stage I caused the pipe to move upward. While α was increasing, the pressure beneath the fixed pipe increased. The best fit curve, given in Fig. 14a, can be used to determine the α value at equilibrium condition. For α = 3.0, the ΔP was zero; thus, the pipe was in equilibrium condition (no

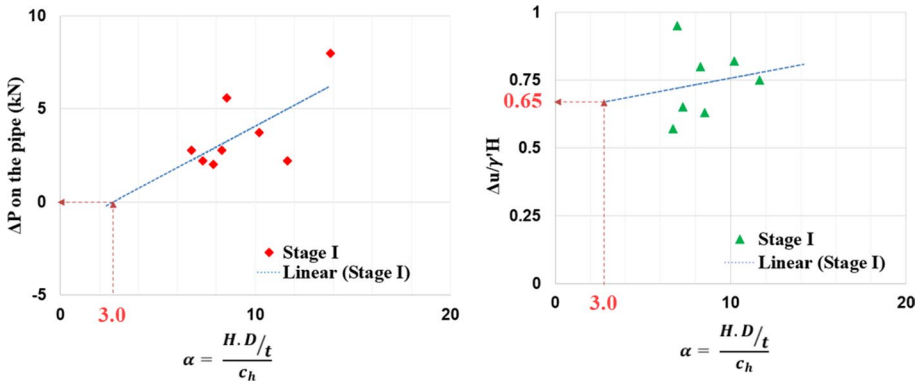

Fig. 14 At different non-dimensional parameter α; **a** ΔP on the fixed pipe and **b** pore pressure ratio

movement). When $\alpha > 3.0$, there was a positive pressure beneath the pipe. As a result, for different depths, pipe diameters, coefficients of consolidation (which represents the GR percentage and size), and uplift starting times, $\alpha < 3.0$ prevents the pipe uplift.

Figure 14b shows the variation of the pore pressure ratio with α. Liquefaction was observed only in clean sand (r_u around 1.0). Although liquefaction was not seen in the SGR mixture, the pipe's upward pressure was due to the developed excess pore water pressure in the mixture. While α was increasing, the pore pressure ratio increased. The best fit curve given in Fig. 14b, can be used to determine the pore pressure ratio at equilibrium condition; it was $0.65 \times \gamma_m^{'} \times H$ for $\alpha = 3.0$.

Based on the findings, the following procedure can be used to decide the burial depth (H) of the pipe in the SGR mixture if the diameter of the pipe (D) is predetermined. Several parameters affect the pipe uplift. Saeedzadeh and Hataf (2011) investigated the effects of dilatancy angle and density ratio of natural soil, diameter and burial depth of the pipe, underground water table, and thickness of the saturated soil layer on the uplift of pipe. They showed the double effect of excess pore water pressure generation, which simultaneously increased the buoyancy force and decreased the effective stress of soil. The pipe uplift was resisted by its deadweight and the effective weight of the above soil. The forces acting on the pipe are illustrated in Fig. 15. The downward force induced by the weight of the SGR mixture above the pipe before shaking is calculated as follows (Chian and Madabhushi 2012):

$$F_m = \left(H \cdot D - \frac{\pi D^2}{8} \right) \gamma_m^{'} \tag{2}$$

where D is the pipe diameter, H is the pipe installation depth in the mixture, and γ'_m is the submerged unit weight of the mixture. At the end of stage I, the downward force induced by the weight of the SGR mixture above the pipe is calculated as

$$F_m = \left(H \cdot D - \frac{\pi D^2}{8} \right) \gamma_m^{'} - \Delta u \cdot D \tag{3}$$

The downward force induced by the deadweight of the pipe is calculated as

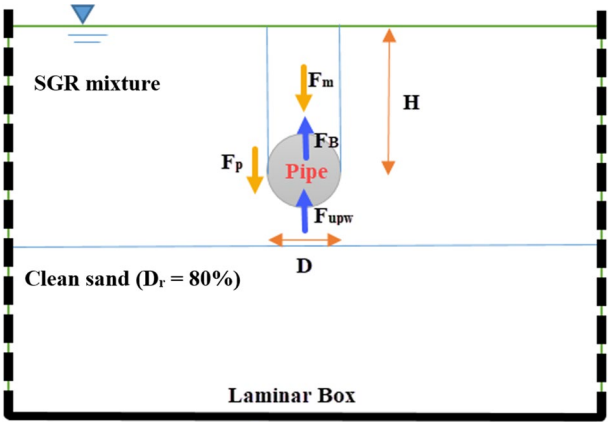

Fig. 15 Downward and upward forces acting on the pipe

$$F_p = \pi\left(bD - b^2\right)\gamma_p \tag{4}$$

where b is the thickness of the pipe and γ_p is the unit weight of the pipe material. The Archimedes principle governs the buoyant force of the structure (F_B). This buoyancy force is determined from the displaced water volume multiplied by the unit weight of the water where the structure is submerged:

$$F_B = \left(\frac{\pi D^2}{4}\right)\gamma_w \tag{5}$$

From the force-balance equation, the forces above the mixture after shaking need to be equal to the pore-water pressure generated at the bottom of the pipe:

$$\left[\left(H \cdot D - \frac{\pi D^2}{8}\right)\gamma_m^{'} - \Delta u \cdot D\right] + \pi\left(bD - b^2\right)\gamma_p - \left(\frac{\pi D^2}{4}\right)\gamma_w = \Delta u \cdot D \tag{6}$$

$$\left[\left(H \cdot D - \frac{\pi D^2}{8}\right)\gamma_m^{'} + \pi\left(bD - b^2\right)\gamma_p - \left(\frac{\pi D^2}{4}\right)\gamma_w\right] = 2\Delta u \cdot D \tag{7}$$

For given dynamic loading and soil conditions, there should be a critical (minimum) pore water pressure that does not cause uplifting of the pipe. In this study, it was found that the uplifting of the pipe occurred as soon as the value of the $\Delta u \geq 0.65 \times \gamma_m^{'} \times H$. Therefore, during the dynamic loading, just before the flotation, the design of the critical condition can be determined as

$$\left[\left(H \cdot D - \frac{\pi D^2}{8}\right)\gamma_m^{'} + \pi\left(bD - b^2\right)\gamma_p - \left(\frac{\pi D^2}{4}\right)\gamma_w\right] \geq 1.3\gamma' \cdot H \cdot D \tag{8}$$

The proposed equation shows that the limits of movement depend strongly on the pipe and backfill material, as well as the installation depth and diameter of the pipe.

6 Conclusions

Pipes that are buried at a shallow depth may be vulnerable to uplift during liquefaction. Several major earthquakes have illustrated this issue. However, the effectiveness of SGR mixture remediation around pipes can enable engineers to design highly secure pipelines in liquefied sites. In this study, to contribute to this development, 13 shaking table tests were performed to examine the seismic-response characteristics of SGR mixtures and the use of these mixtures as a remedial measure to mitigate the forces coming to pipelines during and after the liquefaction. The significant findings obtained from the experimental program are as follows:

1. During shaking, the effective stress decreased due to the generation of significant pore-water pressure in clean sand. However, the Δu generation decreased with increasing volume of the highly deformable GR within the clean sand. As a result, an SGR mixture can prevent the liquefaction phenomenon.

2. When the pipes were placed in the SGR mixture, the GR attenuated the amplitudes of the dynamic waves, efficiently isolating the pipe from the dynamic waves propagating from the bottom of the soil.
3. Generally, in SGR mixtures, the increase in the pore water pressure ratio is lower than that observed in the clean sand. Here, when the SGR mixture was placed as a backfill around the pipe, the excess pore water pressure dissipated more quickly after shaking. In mixtures with a GR ratio of 30 percent, no liquefaction occurred.
4. The excess pore pressure ratio and pipe uplift at different GR dimensions and ratios indicate no clear correlation. Therefore, as an alternative to the GR dimension and ratio, the combination of pipe diameter (D), burial depth (H), consolidation coefficient (c_h) of the mixture, and uplift initiation time (t) was used to develop a non-dimensional parameter (α), which represented a wider range of situations. In this study, the coefficient of consolidation (c_h) was the only variable. For $\alpha = 3.0$, the load increment below the pipe was zero; thus, the pipe was in equilibrium condition.
5. The backfill and pipe density should be sufficient to balance the developed uplift forces on buried pipelines during earthquakes. Placing sheets of clean GR at the bottom of the sand deposits can represent a more substantial design for preventing the liquefaction phenomenon instead of having the same size and volume of GR mixed with the sand to generate the backfill. This can be investigated in subsequent studies.

Acknowledgements The authors are grateful for the financial support provided by the Scientific and Technological Research Council of Turkey (TUBITAK—Project No: 215M402).

References

Anastasiadis A, Senetakis K, Pitilakis K (2012) Small-strain shear modulus and damping ratio of sand-rubber and gravel-rubber mixtures. Geotech Geol Eng, 30(2):363–82. DOI: https://doi.org/10.1007/s10706-011-9473-2

ASTM D3441 (2016) Standard test method for mechanical cone penetration testing of soils. DOI: https://doi.org/10.1520/D3441-16

ASTM D6270–98 (1998) Standard practice for use of scrap tires in civil engineering. ASTM, W. Conshohocken, PA.

ASTM D6270–08 (2012) Standard practice for use of scrap tires in civil engineering applications. ASTM: D6270–08 (Reapproved, 2012). DOI: https://doi.org/10.1520/D6270-08R12.2

ASTM D854-14 (2014) Standard test methods for specific gravity of soil solids by water pycnometer. ASTM International, West Conshohocken, PA

Attom MF (2006) The use of shredded waste tires to improve the geotechnical engineering properties of sand. Envion Geol 49:497–503. https://doi.org/10.1007/s00254-005-0003-5

Bahadori H, Manafi S (2014) Effect of tyre chips on dynamic properties of saturated sands. Int J Phys Model Geotech. https://doi.org/10.1680/ijpmg.13.00014

Bosscher PJ, Edil TB, Eldin NN (1992) Construction and performance of a shredded waste-tire test embankment. Transportation Research Record No. 1345; Transportation Research Board, Washington, D.C., USA, 44–52.

Castiglia M, Santucci de Magistris F, Koseki J (2019) Uplift of buried pipelines in liquefiable soils using shaking table apparatus. In 7th International Conference on Earthquake Geotechnical Engineering, ICEGE 2019, 1638–1646. ISBN 978–0–367–14328–2

Castiglia M, Santucci de Magistris F, Morgante S, Koseki J (2020) Geogrids as a Remedial measure for seismic-liquefaction induced uplift of onshore buried gas pipelines. national conference of the researchers of geotechnical engineering, CNRIG 2019: Geotechnical Research for Land Protection and Development, 649–657. DOI: https://doi.org/10.1007/978-3-030-21359-6_69

Chian SC, Madabhushi SPG (2012) Effect of soil conditions on uplift of underground structures in liquefied soil. J Earthquake Tsunami 6(4):1–20. https://doi.org/10.1142/S1793431112500200

CEN Workshop agreement (2002) Post-consumer tyre materials and applications. CWA 14243 - 2002.
Ecemis N (2013) Simulation of seismic liquefaction: 1-g model testing system and shaking table tests. Eur J Environ Civ Eng 17(10):899–919. https://doi.org/10.1080/19648189.2013.833140
Ecemis N, Demirci HE, Karaman M (2015) Influence of consolidation properties on the cyclic re-liquefaction potential of sands. Bull Earthq Eng 13(6):1655–1673. https://doi.org/10.1007/s10518-014-9677-y
Edil TB, Bosscher PJ (1994) Engineering properties of tire chips and soil mixtures. Geotech Test J 7(4):453–464. https://doi.org/10.1520/GTJ10306J
Gotteland P, Lambert S, Balachowski L (2005) Strength characteristics of tire chips-sand mixture. Stud Geotech Mech 27(1):55–66
Hall WJ, O'Rourke TD (1991) Seismic behavior and vulnerability of pipelines. Lifeline earthquake engineering, M. A. Cassaro, ed., ASCE, New York, 761–773.
Hamada M, Isoyama R, Wakamatsu K (1996) Liquefaction-induced ground displacement and its related damage to lifeline facilities. Soils Found 36(Supplement):81–97. https://doi.org/10.3208/sandf.36.Special_81
Hyodo M, Yamada S, Orense RP, Okamoto M, Hazarika H (2008) Undrained cyclic shear properties of tire chip-sand mixtures. In: Proceedings of the international workshop on scrap tire derived geomaterials opportunities and challenges. London: Taylor and Francis; 187–196. ISBN 978–0–415–46070–5
Hazarika H, Hyodo M, Yasuhara K (2010) Investigation of tire chips-sand mixtures as preventive measure against liquefaction. In Ground Improvement and Geosynthetics (Puppala AJ, Huang J, Han J and Hoyos LR (eds)). American Society of Civil Engineers, Reston, VA, USA, ASCE Geotechnical Special Publication 207, 338–345. DOI: https://doi.org/10.1061/41108(381)44
Kaneko T, Rolando PO, Masayuki H, Norimasa Y (2013) Seismic response characteristics of saturated sand deposits mixed with tire chips. J Geotech Geoenviron Eng 139(4):633–643. https://doi.org/10.1061/(ASCE)GT.1943-5606.0000752
Kim HK, Santamarina JC (2008) Sand–rubber mixtures (large rubber chips). Can Geotech J 45(10):1457–1466. https://doi.org/10.1139/T08-070
Lee C, Truong QH, Lee W, Lee JS (2010) Characteristics of rubber-sand particle mixtures according to size ratio. J Mater Civ Eng 22(4):323–331. https://doi.org/10.1061/(ASCE)MT.1943-5533.0000027
Ling HI, Mohri Y, Kawabata T, Liu H, Burke C, Sun L (2003) Centrifugal modeling of seismic behavior of large-diameter pipe in liquefiable soil. J Geotech Geoenviron Eng 129(12):1092–1111. https://doi.org/10.1061/(ASCE)1090-0241(2003)129:12(1092)
Lunne T, Robertson PK, Powell JJM (1997) Cone-penetration testing in geotechnical practice. Taylor and Francis Group, ISBN 10: 0419 23750 X, ISBN 13:978041923750 1
Mahboub KC, Massie PR (1996) Use of scrap tire chips in asphaltic membrane. Transp Res Rec J Transp Res Board 1530(1):59–63. https://doi.org/10.3141/1530-08
Manion WP, Humphrey DN (1992) Use of tire shreds as lightweight and conventional embankment fill. Phase I – Laboratory, Technical Paper 91–1; Technical Services Division, Maine Department of Transportation, Augusta, ME, USA.
Mohri Y, Yasunaka M, Shigeru T (1995) Damage to buried pipeline due to liquefaction induced performance at the ground by the Hokkaido–Nansei–Oki earthquake in 1993. Proc., 1st Int. Conf. on Earthquake Geotechnical Engineering, K. Ishihara, ed., Balkema, Rotterdam, The Netherlands, 31–36.
Mohri Y, Kawabata T, Ling HI (1999) Experimental study on the effects of vertical shaking on the behavior of underground pipelines. Proc 2nd Int Conf on Earthquake Geotechnical Engineering, Lisbon, Portugal, 489–494.
Neaz Sheikh M, Mashiri MS, Vinod JS, Tsang H (2013) Shear and compressibility behavior of sand–tire crumb mixtures. J Mater Civil Eng 25(10):1366–1374. https://doi.org/10.1061/(ASCE)MT.1943-5533.0000696
Noorzad R, Raveshi M (2017) Mechanical Behavior of waste tire crumbs-sand mixtures determined by triaxial tests. Geotech Geol Eng 35:1793–1802. https://doi.org/10.1007/s10706-017-0209-9
Orense RP (2015) Recent trends in ground improvement methods as countermeasure against liquefaction. 6th International Conference on Earthquake Geotechnical Engineering. Christchurch: New Zealand.
O'Rourke MJ, Liu X (1999) Response of buried pipelines subject to earthquake effects. Multidisciplinary Center for Earthquake Engineering Research, Buffalo, N.Y.
Phillips R, Valsangkar AJ (1987) An experimental investigation of factors affecting penetration resistance in granular soils in centrifuge modelling. Technical Report No CUED/D-Soils TR210, Cambridge University, UK.
Promputthankgoon P, Hyde AFL (2010) Liquefaction mitigation by means of sand-tyre chip mixtures, 17th SEAGC, Taiwan, 371–374.
Renzi R, Corte JF, Bagge G, Gui M, Laue J (1994) Cone penetration tests in the centrifuge: experience of five laboratories. In: Proceedings of international conference centrifuge 94, Singapore, 77–82.

Saeedzadeh R, Hataf N (2011) Uplift response of buried pipelines in saturated sand deposit under earthquake loading. J Soil Dyn Earthquake Eng 31:1378–1384. https://doi.org/10.1016/j.soildyn.2011.05.013

Terzi NU, Erenson C, Murat E, Selçuk ME (2015) Geotechnical properties of tire-sand mixtures as backfill material for buried pipe installations. Geomech Eng 9(4):447–464

Thomas BS, Gupta RC (2015) Long term behaviour of cement concrete containing discarded tire rubber. J Clean Prod 102:78–87. https://doi.org/10.1016/j.jclepro.2015.04.072

Uchimura M, Chi NA, Nirmalan S (2007) Shaking table test on the effect of tire chips and sand mixture in increasing liquefaction resistance and mitigation uplift of pipe. International Workshop on Scrap Tire Derived Geomaterials, Yokosuka, Japan

Uchimura T, Chi NA, Nirmalan S, Sato T, Meidani M, Towhata I (2008) Shaking table tests on effect of tire chips and sand mixture in increasing liquefaction resistance and mitigating uplift of pipe. In: Proceedings of the international workshop on scrap tire derived geomaterials—opportunities and challenges. London: Taylor and Francis, 179–86.

Youwai S, Bergado DT (2003) Strength and deformation characteristics of shredded rubber tire-sand mixtures. Can Geotech J 40:254–264. https://doi.org/10.1139/t02-104

Zornberg JG, Cabral AR, Viratjandr CH (2004) Behaviour of tire shred–sand mixtures. Can Geotech J 41:227–241. https://doi.org/10.1139/t03-086

Zou D, Kong X, Xu B. (2006) Numerical simulation of seismic behavior of pipeline in liquefiable soil. In: Proceedings of the geotechnical symposium in Roma: soil stress-strain behavior, measurement, modeling and analysis, 673–82. DOI: https://doi.org/10.1007/978-1-4020-6146-2_48